

# Self-Supervised Representation Learning from Temporal Ordering of Automated Driving Sequences

Christopher Lang<sup>1,2</sup> Alexander Braun<sup>2</sup> Lars Schillingmann<sup>2</sup> Karsten Haug<sup>2</sup> Abhinav Valada<sup>1</sup>  
<sup>1</sup>University of Freiburg <sup>2</sup>Robert Bosch GmbH

## Abstract

Self-supervised feature learning enables perception systems to benefit from the vast amount of raw data being recorded by vehicle fleets all over the world. However, their potential to learn dense representations from sequential data has been relatively unexplored. In this work, we propose TempO, a temporal ordering pretext task for pre-training region-level feature representations for perception tasks. We embed each frame by an unordered set of proposal feature vectors, a representation that is natural for instance-level perception architectures, and formulate the sequential ordering prediction by comparing similarities between sets of feature vectors in a transformer-based multi-frame architecture. Extensive evaluation in automated driving domains on the BDD100K and MOT17 datasets shows that our TempO approach outperforms existing self-supervised single-frame pre-training methods as well as supervised transfer learning initialization strategies on standard object detection and multi-object tracking benchmarks.

## 1. Introduction

Automated driving datasets typically cover only small sets of visual concepts, e.g., eight object classes in BDD100K [56] or ten classes in nuScenes [13], using a fixed camera setup. This narrow perspective can lead to poor transfer abilities, such that models struggle with driving scenes that are weakly represented in the training data [2]. Consequently, very large datasets are required to cover the numerous traffic scenarios, which are expensive to curate and manually annotate. Self-supervised learning approaches offer a promising solution, as they allow network parameters to be pre-trained on pretext tasks that provide free supervision from consistency constraints in the raw data. The design of these pretext tasks should aim to encourage the network to learn rich intermediate representations, that emerge independent of human annotation, and benefit in fine-tuning the network on a downstream task with limited annotated data.

Successful applications of self-supervised learning (SSL)

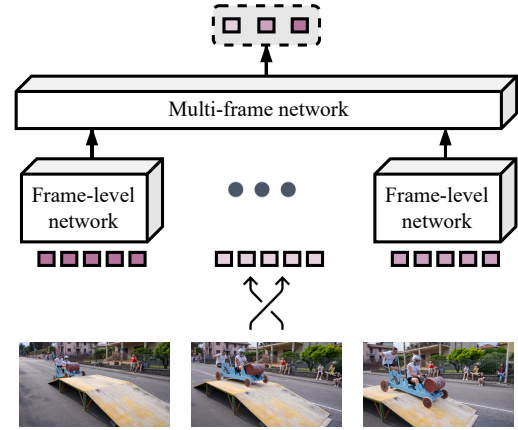


Figure 1. We introduce TempO, a self-supervised learning pretext task by temporal ordering of frames, that pre-trains perception models for both frame-level tasks, like object detection, and multi-frame tasks like multi-object tracking. We propose a transformer-based architecture that is designed to scale quadratic w.r.t. sequence length, and enables richer temporal context during pre-training.

methods as pre-training for image classification tasks have been demonstrated by image-level feature learning using contrastive methods [4–6, 16]. These approaches were later extended to region-level representation learning, where the contrastive approach is applied to image patches tracked over a set of augmentations [8, 52]. In robotic domains, such as automated driving, the perception system observes the environment from a continuous stream of sensor data. Adding such temporal context allows learning from undistorted images by exploiting object permanence and dynamical constraints. Recent methods exploit these by enforcing linear motion models and static scene assumptions for depth estimation [14], or consistent appearance constraints in tracking patches along a temporal cycle [23, 46, 47]. However, such methods fail once these underlying assumptions are violated (e.g. by dynamic objects in the scene or large camera movements), resulting in inconsistent predictions or indefinite loss values. The task of ordering a set of shuffled frames into their original temporal succession by video-level feature representations [26, 33] has shown promising results, as it is less ambiguous and never ill-defined while encouraging

an understanding of both local object semantics and global scene composition.

In this work, we propose *TempO*, a self-supervised representation learning approach that extends temporal ordering to region-level feature learning for object detection and tracking. We achieve this synergy by defining the temporal ordering task as a sequence estimation problem and construct the method based on the tracking-by-detection paradigm, as depicted in Figure 1. This design of a single-frame (spatial) network and a light multi-frame head requires the network to learn consistent representations and perform the bulk of the semantic reasoning for each frame separately. We evaluate the performance of *TempO* pre-training on downstream tasks of object detection on the BDD100K dataset and multi-object tracking on the BDD100K and MOT17 datasets, by comparing with pre-training on supervised datasets and existing unsupervised pre-training methods. Furthermore, we study the utility of representations learned from *TempO* pre-training for the frame retrieval task, without additional training.

The main contributions of this work are:

- We propose *TempO*, a self-supervised pretraining pipeline for object detection models and multi-object tracking models from a temporal ordering pretext.
- We design a transformer-based multi-frame sorting head whose computational complexity scales less than quadratic with the sequence length. This allows us to pretrain on longer sequences compared to combinatorial approaches [33, 53].
- We perform extensive evaluations of *TempO* pre-training for the downstream tasks of object detection and multi-object tracking that demonstrate the utility of our approach.

## 2. Related Work

Our work is related to the field of self-supervised visual representation learning from sequential data. In the following, we embed our proposed method in these areas.

*Self-Supervised Image Feature Learning:* Self-supervised learning has been studied extensively on single images, where the field can be broadly categorized into image-level, region-level, and pixel-level approaches. Image-level approaches learn a global embedding vector per frame and are typically evaluated on image classification tasks. Contrastive methods learn an image feature vector that is invariant to a set of augmentations while being distinct from embeddings of other images. The choice of negative examples ranges from instance-based discrimination [6, 7], clustering-based pretext tasks [4], and bootstrapping approaches [5, 16]. The temporal consistency in video clips is also used as a source for positive pairs from subsequent frames [11]. Enforcing such temporally persistent features benefits both instance-based discrimination and clustering-based methods [11].

Nevertheless, many computer vision tasks, including object detection [24, 25] and segmentation [15, 34, 45], require dense representations that also encode local image information. Region-level approaches [8, 9, 57], therefore, rely on pretext tasks that operate on patches of an image or the feature map. Patch discrimination methods [29, 35] utilize these image patches to learn local augmentation-invariant embeddings, analogously to the image-level methods described above. The patch re-identification pretext task [10, 19], on the other hand, emphasizes the localization task by regressing the image coordinates of the local patch in the global image. Combining patch discrimination and re-identification pretext tasks have shown sustainable gains for downstream object detection [8, 10, 51, 52], as the losses include regression and classification-based terms analogously to the downstream task. In our experiments, we compare against *UP-DETR* [8] as a baseline, which is trained on localizing random crops in an image and contrasting the feature embeddings of crops within an image. It, therefore, is less sensitive to the choice of image augmentations, which is comparable to our proposed method. Dense self-supervised feature learning approaches on the level of pixels [35, 38, 52] or features [29, 48, 54] are evaluated on segmentation tasks. The pretext tasks rely on unsupervised segmentation masks [19, 20] or the construction of new images [48, 54, 55].

In recent years, consistency constraints in sequential data have been used as a supervisory signal to learn dense feature representations. Tracking approaches exploit object permanence constraints in appearance by searching image patches by their representation in a feature map. The pretext task is either to predict the offset of an image region forward and then backward along a cycle in time [21, 47], whereby the difference between start and end points is used as a training signal. However, such methods operate only on pairwise frame contexts and depend on data domains where the presence of an object over a certain time window can be ensured. Cross-stream approaches [17, 43, 44] estimate the optical flow between two images, from which they derive an informed selection of positive and negative patches [43], instances [17] or prototypes [44] for contrastive learning.

*Self-Supervised Video Feature Learning:* Video feature learning exploits the temporal consistency in sequential data as a supervision signal to generate video-level embeddings. Self-supervised learning approaches can be broadly categorized into three types of pretext tasks: 1. Video discrimination learns contrastive video-features [9, 11, 39] that are invariant to a set of temporally consistent augmentations. 2. Sequential verification performs a binary classification if either a sequence is incorrect or in a shuffled temporal order [12, 33]. Other formulations discriminate between forward and backward order of frames [49]. Such methods are used for encoding video clips all at once but are outper-

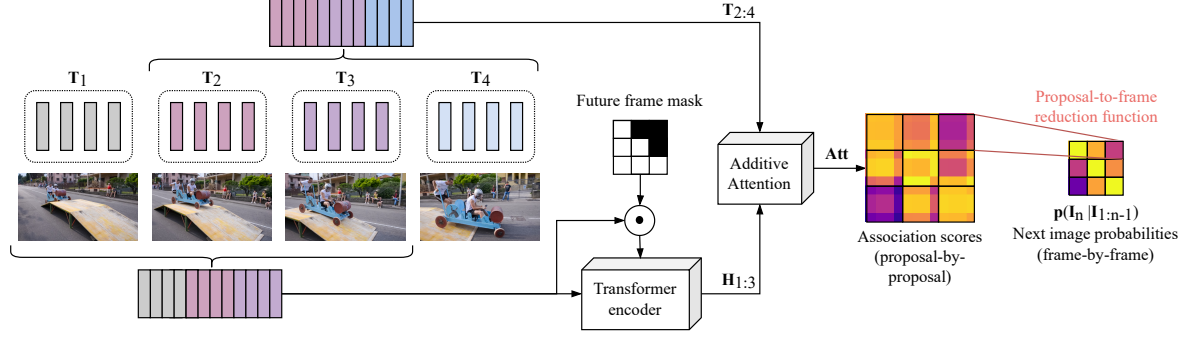


Figure 2. Illustration of the multi-frame head in the *TempO* architecture. Each frame  $n$  is represented by a set of proposal feature vectors  $\mathbf{T}_n$  extracted by the same frame-level network. The proposal features are concatenated and encoded by a transformer encoder into a set of history tokens  $\mathbf{H}$  using a future frame masking that allows for each proposal to aggregate temporal context from past frames only. An additive attention mechanism then computes the association scores between the history tokens and the proposal feature vectors. We next map all scores of proposal features corresponding of the same frame onto scalar image transition probabilities. Our proposed temporal ordering task maximizes these probabilities for the correct temporal order during pre-training.

formed by temporal ordering methods as the network needs to reason and understand the statistical temporal structure of image sequences 3. Temporal ordering methods on video classification tasks [26, 37, 49] is formulated as a classification problem among all the frame permutations, which limits their usage to sequence lengths of usually not more than six frames due to the combinatorial explosion of orderings. While the aforementioned methods learn video-level embeddings, they are widely evaluated on clip retrieval and action recognition tasks. We define the temporal ordering pretext task as a sequence estimation problem by estimating image transition probabilities instead of a multi-classification problem, which allows learning frame-level feature representations that allow for a larger variety of downstream tasks, as described in the following section.

### 3. Technical Approach

We next detail our proposed *TempO* pretext task for region-level visual representation learning. In the remainder of this section, we first introduce the pretext task in Section 3.1, followed by the network architecture in Section 3.2 and Section 3.3, and finally describe the transfer learning technique to perform downstream task evaluations in Section 3.4.

#### 3.1. Sequence Ordering Task Definition

For the *TempO* pretext task, we consider image sequences of length  $N$ . We chose the starting index such that  $n = 1, \dots, N$  for a more concise notation. A training sample is composed of the first frame in the sequence  $\mathcal{I}_1$  as an anchor in time, and the remaining sequence frames  $\mathcal{I}_{2:N}$  in arbitrary order. At first, a single-frame network extracts an unordered set of proposal feature vectors from each frame independently. The multi-frame transformer head then processes the concatenated proposal feature vectors over all  $N$  frames in a training sample and maps them onto next-image probabilities given a sequence of images as described in Section 3.3.

Our training objective is to maximize the next-image probability  $\rho(\mathcal{I}_n | \mathcal{I}_{1:n-1})$  for the observed temporal orderings in the video data using a ranking loss formulation

$$\mathcal{L} = \sum_{m \neq n} \max \{ \rho(\mathcal{I}_m | \mathcal{I}_{1:n-1}) - \rho(\mathcal{I}_n | \mathcal{I}_{1:n-1}) + \Delta, 0 \}, \quad (1)$$

where  $\Delta \geq 0$  is a scalar margin.

#### 3.2. Single-Frame Network

Our approach adapts to network architectures that process images and produces a set of  $P$  proposal feature vectors  $\mathbf{Q} \in \mathbb{R}^{P \times D}$  of dimension  $D$  per frame. This includes common region proposal-based [42] and transformer-based [3, 58] architectures. The majority of our experiments are conducted on the *Sparse R-CNN* [42] object detection architecture, using a ResNet-50 [18] as a feature extractor. It learns a sparse set of  $P$  proposal boxes and features, from which classification scores and bounding boxes are generated. The initial proposal features are extracted from learned proposal box regions in the feature map. The proposal features are then iteratively refined by a sequence of dynamic heads that each allow interaction between proposal features via self-attention modules.

We implement two distinct branches of dynamic heads: a detection branch that extracts object proposal features, consisting of six iterative heads, and a tracking branch that extracts tracking proposal features, from two iterative dynamic heads, that are used to associate objects identities throughout a sequence. The model under pre-training uses two dynamic heads, whose parameters are cloned to initialize the parameters of both the detection and tracking branch (see Section 3.3) during fine-tuning. The motivation for separating the tracking and detection branches is that the feature representations pursue competing objectives. While detection features should learn to generalize across an object type (e.g. car), tracking features should learn to discriminate between object instances.

### 3.3. Multi-Frame Sequence Ordering Network

The overall setup of our sequence ordering network is depicted in Figure 2. We express the image transition probability with respect to the track features as  $\rho(\mathcal{I}_n | \mathcal{I}_{1:n-1}) = \rho(\mathbf{T}_n | \mathbf{H}_{n-1})$  given a set of sequence history up to frame  $n - 1$  as  $\mathbf{H}_{n-1} \in \mathbb{R}^{(P \times D)}$ . The history tokens at  $\mathbf{H}_{n-1}$  are the output sequence tokens by a transformer encoder, that takes as input the track feature vectors up to frame  $n - 1$ . This is implemented by masking track features of future frames in the attention matrix.

Finally, we compute additive attention between the encoded sequence history tokens and the track features given by

$$Att(\mathbf{t}_n^i, \mathbf{h}_m^j) = \mathbf{v}^T \tanh(\mathbf{W}_1 \mathbf{t}_n^i + \mathbf{W}_2 \mathbf{h}_m^j), \quad (2)$$

where  $Att(\mathbf{t}_n^i, \mathbf{h}_m^j)$  denotes the attention score between  $\mathbf{t}_n^i$ , i.e., the  $i$ -th proposal vector in frame  $n$ , and  $\mathbf{h}_m^j$ , i.e., the  $j$ -th history feature vector up to frame  $m$ .  $\mathbf{v}$ ,  $\mathbf{W}_1$ , and  $\mathbf{W}_2$  are the learnable parameter matrices. In the next step, we employ a reduction function that computes a scalar ordering score from the track-to-history association score matrix.

*Proposal-to-Frame Reduction Function:* The final stage in our multi-frame head is the reduction from an association score matrix to a next-frame transition probability. As the associations are derived from unordered sets of proposals, this function is required to be permutation invariant with respect to the elements of the association matrix. One naive candidate is the mean over all matrix elements (*AvgPool*) that encourage similarity between all track features in temporally subsequent frames. Since tracking requires a consistent embedding of an object across subsequent frames, we also experiment to enforce a one-to-one matching among track features of two frames. Therefore, we propose an approximation of the linear sum assignment, as follows:

$$\rho(\mathbf{T}_n | \mathbf{H}_m) = \sum_j \max_i \left[ \text{softmax}_{i=1, \dots, P} (Att(\mathbf{t}_n^i, \mathbf{h}_m^j)) \right] \quad (3)$$

and ablate over these choices of the reduction function.

### 3.4. Downstream Task Architectures

Our models use the ResNet-50 [18] architecture as the backbone and the Sparse R-CNN [42] architecture with two iterative dynamic heads for generating 100 object proposals per frame. The ResNet-50 parameters are initialized with weights pre-trained on the ImageNet dataset and all the other model parameters are randomly initialized. For the pretext task, we collect feature vectors over all sequence frames and feed them to a masked transformer encoder described in Section 3.3. Since we exclusively use permutation invariant operations and no positional embedding on the multi-frame level, we omit the explicit shuffling of frames in our implementation.

*Object Detection:* For the object detection fine-tuning, we adapt the originally proposed Sparse R-CNN configuration [42]. Therefore, we build upon the pre-trained Sparse R-CNN architecture and stack four iterative dynamic heads on top of the pre-trained heads, called the detection branch. The final object proposal vectors are mapped onto classification scores and bounding box regression coordinates using separate linear layers.

*Multi-Object Tracking:* During the Multi-Object Tracking (MOT) downstream task, we associate proposals based on their additive attention between track features  $\mathbf{T}_i$  and the history features of the previous frame  $\mathbf{H}_{i-1}$  that is generated by the transformer encoder. We follow the setup in *QD-Track* [36], applying their bidirectional softmax matching in feature space, tracker logic, and training pipeline. We further extend the model into an object detector, as described above. We, therefore, clone the pre-trained iterative heads, such that they have distinct parameter sets for the tracking and detection branch.

## 4. Experimental Results

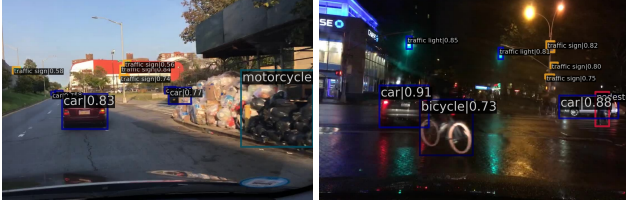
We pre-train the networks using our proposed *TempO* approach on the train splits of the Berkeley Deep Drive [56] (BDD100K) as well as MOT17 [32] (MOT17) datasets. In this section, we compare the performance of *TempO* pre-trained models with other initialization strategies from the literature for single-frame as well as multi-frame downstream perception tasks.

### 4.1. Datasets

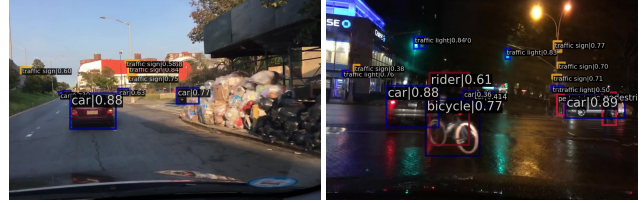
The Berkeley Deep Drive [56] (BDD100K) dataset contains crowdsourced videos of driving scenes such as city streets and highways. It consists of different weather conditions and times of the day. For MOT fine-tuning, we use the annotations of the BDD100K and MOT17 images at 5 frames per second (FPS), which consist of 1400 videos of 40 s length. The annotations cover eight object categories of overall 131k identities. For object detection fine-tuning, we use annotations from the object detection challenge, which provides eight annotated categories for evaluation. The MOT17 [32] (MOT17) challenge consists of 14 video sequences (7 training, 7 test) at varying frame rates ( $>14\text{fps}$ ) and sequence lengths ( $>20\text{s}$ ) in unconstrained environments filmed with both static and moving cameras. It provides MOT annotations that feature a people class with at least three persons visible per frame. For our pre-training, we sample frames at 5 FPS from videos in the training split, from which we generate non-overlapping training sequences.

### 4.2. Training Protocol

We train the models on NVIDIA V100 GPUs with a batch size of 8 for 6 epochs on the pretext tasks. We use the



(a) ImageNet initialized, trained for 12 epochs on BDD100K



(b) *TempO* pre-trained, fine-tuned for 6 epochs on BDD100K.

Figure 3. Qualitative object detection results on the BDD100K val set using the Sparse R-CNN detector with varying training schedules. Observe that the *TempO* pre-trained detector avoids a ghost detection of a motorcycle within the garbage bags and detects the poorly lit rider on top of the moving bicycle.

AdamW optimizer with an initial learning rate of  $2.5 \cdot 10^{-5}$  and weight decay of  $10^{-4}$ . A step scheduler further reduces the learning rate by a factor of 10 every 3 epochs. We fine-tune the models for another 6 epochs on the respective downstream tasks. The baselines were trained for 12 epochs on the downstream tasks, such that all models have seen each frame at most 12 times during training. We resize the images to a resolution of 800 pixels on the longer side and perform random cropping (spatial augmentation) or photometric augmentations such as color jitter, random gray scaling, and brightness change, only when stated.

### 4.3. Evaluations on Downstream Tasks

We evaluate how the region-level feature representations learned from the *TempO* pre-training impacts the performance of single-frame and multi-frame downstream tasks, i.e., for object detection and multi-object tracking on the BDD100K as well as the MOT17 dataset. We follow the evaluation protocol as in [5, 7, 53], where we fine-tune all models for the same fixed number of epochs (12 in our case). The *TempO* pre-training consists of ordering sequences of length  $N = 8$ , using two layers in the transformer encoder, for 6 epochs, followed by fine-tuning on the downstream task for another 6 epochs.

#### 4.3.1 Object Detection Results

Table 1 shows the mean average precision over all the classes in the BDD100K object detection benchmark. The average precision measures the area under the precision-recall curve for detections averaged over thresholds for  $\text{IoU} \in [0.5 : 0.05 : 0.95]$  with the ground truth bounding boxes. We compare our proposed SSL pre-training approach against various initialization strategies using the Sparse R-CNN [42] object detector, including the common practice of pre-training the feature extractor as a classifier on the ImageNet dataset, as well as pre-training the model parameters on the supervised Common Objects in Context [28] (COCO 2017) object detection dataset. Additionally, we compare against the single-frame self-supervised pre-training task of random query patch detection (RPD) as described in [8]. For our adaptation to the Sparse R-CNN detector, we add the

Table 1. Object detection results on the BDD100k val dataset. We use a sequence length of 8 frames in the *TempO* pre-training, two layers in the multi-frame network, and AvgPool motivated by the ablation results presented in Table 3.

Pre-train Method	Model	BDD100k val object detection					
		AP	AP50	AP75	APs	APm	API
ImageNet	Faster R-CNN	23.1	45.7	20.2	10.0	28.0	38.8
	FCOS	25.9	46.7	24.5	7.6	31.2	52.0
	Sparse R-CNN	24.9	46.8	<b>31.3</b>	10.7	31.2	42.4
RPD	Sparse R-CNN	29.4	54.3	27.2	14.3	32.8	49.1
COCO	Sparse R-CNN	30.7	55.8	28.9	15.2	34.3	50.8
	DeformableDETR	30.2	56.0	27.6	14.2	34.0	51.3
<i>TempO</i>	Faster R-CNN	24.3	49.1	21.8	12.6	30.3	42.1
	DeformableDETR	30.8	56.9	28.4	14.5	34.9	<b>53.8</b>
	Sparse R-CNN	<b>31.4</b>	<b>57.3</b>	29.5	<b>15.7</b>	<b>35.2</b>	51.6

patch image features to the initial proposal features of the Region Proposal Network (RPN) neck.

We observe that our *TempO* initialization outperforms supervised pre-training on the COCO 2017 dataset by  $+0.7\%mAP$ , while the performance gain compared to the single-frame pretext task of random query patch detection is as large as  $+2\%mAP$  evaluated using the Sparse R-CNN detector. Moreover, *TempO* pre-training results in faster convergence of the detectors. Please refer to the supplementary material for a comparison of convergence plots. In Figure 3, we present qualitative results of (a) a Sparse R-CNN object detector trained with ImageNet pre-trained weights and (b) the *TempO* pre-trained Sparse R-CNN detector. Compared to the fully supervised training strategy, the *TempO* pre-trained Sparse R-CNN detector improves detection accuracy as it suppresses a ghost detection of a motorcycle within the pile of garbage bags on the right side of the image shown in Figure 3 (b). It also detects the poorly illuminated rider on top of the moving bicycle in Figure 3 (b).

#### 4.3.2 Multi-Object Tracking Results

We evaluate our *TempO* pre-trained models on the MOT downstream task using the standard evaluation metrics [22]. We build on QDTrack [36] to extend our model into a multi-object tracker, as it associates detected objects in the feature

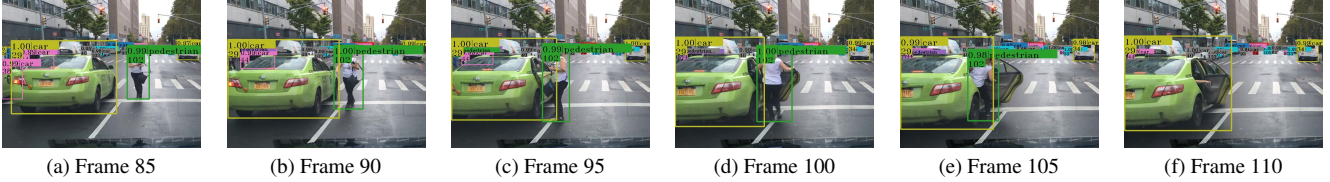


Figure 4. Qualitative MOT results on BDD100K validation set for our proposed transformer tracking architecture and pre-trained on a sequential ordering task. The network tracks the pedestrian reliably over changing body orientations and handles the changing shape of the green car.

Table 2. Multi-object tracking performance evaluation on BDD100k val set.

Model	Detector	Initialization	BDD100k val						
			HOTA $\uparrow$	DetA $\uparrow$	AssA $\uparrow$	LocA $\uparrow$	MOTA $\uparrow$	IDF1 $\uparrow$	IDS <sub>w</sub> $\downarrow$
QD Track	Faster R-CNN	BDD100k	38.3	38.4	<b>39.6</b>	68.5	29.3	<b>49.7</b>	<b>90590</b>
QD Track	Sparse R-CNN	BDD100k	37.2	38.2	32.3	69.5	28.7	43.9	94688
TempO	Sparse R-CNN	TempO	36.6	35.2	30.1	66.1	26.3	40.1	108755
TempO	Sparse R-CNN	TempO+BDD100k	<b>39.2</b>	<b>39.6</b>	38.7	<b>69.6</b>	<b>31.2</b>	46.8	91083

space and is the current state-of-the-art on the BDD100K MOT benchmark for models with fewer than 100M parameters. As a baseline, we trained this method in its standard configuration using the Faster R-CNN and Sparse R-CNN model as a detector, which was pre-trained on the BDD100K detection dataset.

Table 2 shows the performance on the BDD100K MOT val dataset for fine-tuning with various parameter initialization strategies on the BDD100K MOT training annotations for 4 epochs. We compare the performance with the higher-order tracking accuracy [31] (HOTA) metric which combines the detection, association, and localization accuracy into a single value. Additionally, we present the benchmark metrics of MOTA, IDF1, and ID switches. We observe that our tracking approach with *TempO* pre-training and prior fine-tuning as an object detector achieves the highest tracking accuracy in both the HOTA and MOTA scores, outperforming the baseline QDTrack using a Faster R-CNN detector by +0.9% in the HOTA score. Interestingly, the Sparse R-CNN approach achieves lower association accuracy and IDF1 scores compared to the Faster R-CNN as a base detector, when only pre-training the object detector, while detection and localization accuracy are at comparable levels. This results in lower overall tracking accuracy when the network parameters are only initialized with *TempO* pre-training, and fine-tuning of both detection and association task are required during the fine-tuning epochs.

Figure 4 shows an example tracking sequence using the tracking architecture described in Section 3.4. We see that the network reliably tracks the car with high confidence, even under heavy occlusion and changing shape from opening the car door. The pedestrian entering the car is successfully tracked over the front, side, and rearview and partially occluded when stepping into the backseat.

**MOT17 Results:** We further evaluate our *TempO* pre-training

strategy on the popular MOT17 benchmark. We pre-trained our model on MOT17 dataset for 50 epochs and compare it against various baselines that are initialized with pre-trained object detectors on the COCO 2017 dataset and with unsupervised pre-training on the Crowdhuman dataset by an RPD pretext task. We follow the training setting described in *QDTrack* and fine-tune our models for 12 epochs on a mixed dataset of CrowdHuman [40] and MOT17 train set. The result in Table 4 shows that *TempO* pre-trained Sparse R-CNN model outperforms both its unsupervised COCO and unsupervised RPD initialized counterparts by +1.4% HOTA and +2.3% MOTA, which mainly trace back to an increased detection accuracy DetA and fewer ID switches.

#### 4.4. Ablation Study

Table 3 shows the benchmarking results for object detection and MOT downstream tasks on the BDD100K val dataset for models pre-trained on our proposed *TempO* training with varying hyperparameter settings. In particular, we ablate over the sequence length, the attention hierarchies of the multi-frame transformer encoder, as well as the choice of temporally-varying frame augmentations.

**Sequence Length:** By varying the number of subsequent frames from 4 to 8, the bounding box AP increases from 31.0% to 31.4%, which suggests that a longer temporal context allows the model to learn more distinctive object attributes to reliably detect object types. For MOT performance, the gain from observing longer sequences and therefore more framewise comparisons are as high as +3% in HOTA

**Hierarchical Attention:** Another vital design aspect is the size of the multi-frame network, and especially the hierarchy of associations that can be increased by stacking multiple encoder layers. The ablation study shows that this

Table 3. Ablation experiments on down-stream tasks for various TempO pre-training settings. All experiments use a Sparse R-CNN object detector with a ResNet-50 backbone and 100 proposals per frame.

$N_{seq}$	Pretext setting			BDD100k val object detection							BDD100k val MOT			
	$L_{\{enc,dec\}}$	$f_{sim}$	Augment.	AP	AP50	AP75	APs	APm	API	HOTA $\uparrow$	sMOTA $\uparrow$	IDF1 $\uparrow$	IDS <sub>w</sub> . $\downarrow$	
4	2	AvgPool	-	31.0	56.5	29.0	15.2	34.8	51.5	33.6	25.5	37.5	102261	
6	2	AvgPool	-	31.2	56.8	29.3	15.3	35.0	51.4	34.9	25.0	36.4	101723	
8	2	AvgPool	-	<b>31.4</b>	<b>57.3</b>	<b>29.5</b>	<b>15.7</b>	<b>35.2</b>	<b>51.6</b>	36.6	26.3	40.5	90388	
8	1	AvgPool	-	29.1	54.1	26.9	14.2	33.1	48.0	35.1	24.4	36.1	92529	
8	4	AvgPool	-	30.9	56.5	28.7	15.2	34.8	50.7	<b>37.2</b>	<b>27.2</b>	<b>42.9</b>	<b>89083</b>	
8	2	AvgPool	P	31.3	56.9	29.3	15.4	35.1	51.2	35.5	15.8	41.5	92053	
8	2	MSA	-	30.7	55.9	29.0	15.1	34.4	25.1	35.3	25.9	40.4	91600	

Table 4. Multi-object tracking performance evaluation on MOT17 test set.

Method	Detector	Initialization	MOTA $\uparrow$	IDF1 $\uparrow$	HOTA $\uparrow$	DetA	AssA	LocA	FP $\downarrow$	FN $\downarrow$	IDs $\downarrow$
QDTrack [36]	Faster R-CNN	COCO	68.7	<b>66.3</b>	53.9	-	-	-	26589	146643	3378
QDTrack	Sparse R-CNN	COCO	69.5	63.4	52.9	56.2	49.1	82.2	21963	147291	3305
QDTrack	Sparse R-CNN	RPD [8] + Crowdhuman	70.8	65.9	52.1	56.7	48.4	80.7	42855	117402	4563
QDTrack	DDETR	TempO + Crowdhuman	72.1	63.9	53.2	57.9	49.1	82.4	18513	135687	3180
QDTrack	Sparse R-CNN	TempO + Crowdhuman	<b>72.8</b>	65.9	<b>54.3</b>	<b>58.5</b>	<b>50.3</b>	<b>82.5</b>	<b>17646</b>	<b>133059</b>	<b>3093</b>

hyperparameter has a big impact on the performance of the downstream task compared to the sequence length. Surprisingly, we find that the complexity is saturated at two encoder layers, while a higher number of layers decreases performance, especially on single-frame object detection tasks. We initially hypothesized that the multi-frame model could be incapable of generalizing across all the dynamic interactions that inform about temporal sequences in traffic scenes. However, the results show that a lighter multi-frame head loads more of the semantic reasoning onto the single-frame model, which thereby learns more expressive features. Moreover, the damped performance can result from the slower convergence due to the high parallelism in multi-head attention modules, such that longer pre-training schedules can be required. Furthermore, using (3) as a reduction function for the association score matrices resulted in a drop in performance compared to average pooling by  $-0.7\%mAP$ , which can be attributed to the sparser and attenuated gradients.

*Spatial and Photometric Augmentations:* In Table 3, we evaluate spatial and appearance-based augmentations of the input sequence. This enforces the network to learn object representations, that are invariant to the global image location or lightning effects. Interestingly, photometric augmentations during pre-training resulted in lower performance on the downstream task, reducing the object detection performance by  $-0.1\%mAP$  and tracking performance by  $-1.4\%HOTA$  for identical TempO settings. This shows that the network exploits internal appearance consistency assumptions. Spatial augmentations such as random cropping negatively affect the pre-training, which indicates that the network relies on consistent spatial cues to solve the temporal ordering task.

Table 5. Frame retrieval experiments on UCF101 [41] dataset.

Method	Model	Top-1	Top-5	Top-10	Top-20
MSE	-	13.1	20.2	23.4	28.6
JigSaw [1]	3D CNN	19.7	28.5	33.5	40.0
OPN [27]	3D CNN	19.9	28.7	34.0	40.6
CCL [23]	3D ResNet	32.7	42.5	50.8	61.2
TempO	Faster R-CNN	34.9	46.1	53.6	58.9
	Sparse R-CNN	<b>35.6</b>	<b>49.5</b>	<b>58.2</b>	<b>68.3</b>
	DDETR	33.1	18.4	56.4	65.9

## 4.5. Frame Retrieval Results

We further evaluate the utility of the learned representations from our TempO pre-training approach for the frame retrieval task on the UCF101 dataset [41], without additional fine-tuning on the retrieval task. We trained models for 100 epochs on the UCF101 videos using the TempO pretext task described in Section 3.1. For frame retrieval, we follow the experimental setup described in [23], by extracting 10 equally distanced frames from each video from the UCF101 dataset and using the frames extracted from videos in the test set, as class representatives. The frames are then classified using nearest-neighbor (NN) search in the embedding space, where closeness is defined by set-similarities as given by average pooling. The frames extracted from the train split clips are queried for similarity with all these class representatives and marked as correctly classified if a vector of the same action class is within the  $k$  nearest neighbors.

We compare against the baseline performances reported by Kong et al. [23]. Table 5 shows the retrieval performance measured as the accuracy for  $k = 1$  to  $k = 20$ . The results demonstrate that the TempO pre-trained embeddings



Figure 5. Frame retrieval demonstrations of misclassifications in the Top-20 setting. Scores are normalized similarities of the Top-20 nearest neighbors. Retrieved frames resemble in scene attributes, for instance the number and size of foreground objects or camera perspective, while backgrounds vary widely.

show strong consistency across videos of the same action class. Interestingly, the similarity is higher than that obtained from other frame-level pre-training strategies, improving the *Top - 1* accuracy by +3.9% compared to the cycle-consistency pretext (CCL) task. In Figure 5, we present examples of misclassified frames and their top three most similar class representatives. We observe that the learned *TempO* representations in these examples focus primarily on similarity of scene attributes, for instance, the number and size of objects or camera perspective. Especially in the example on the bottom row in Figure 5, the large variety of backgrounds indicates that the learned representation consists more of tracking features on foreground objects.

#### 4.6. Discussion of Limitations

Our analysis, and the SSL video feature learning field in general, focuses on relatively short clips  $< 2s$ . Many actions in automated driving or human activity recognition, however, extend over longer time periods, and also our ablation study suggests that longer sequences can benefit the pre-trained models. The integration of more efficient video architectures, *e.g.* on compressed videos [50], would be an important enabler to consider longer time intervals. In our design, however, the association of objects over an increased number of frames can become computationally expensive, which can be alleviated by sampling a subset of frames to be compared. Secondly, we do most of our evaluation on driving sequences, where the camera moves smoothly in a dynamic environment. We chose this domain as the BDD100K

dataset provides many hours of videos with high variability, as well as object detection and multi-object tracking annotations without domain shift. Even though we also evaluate on MOT17 and UCF101 [41] (UCF101) datasets, which are more human-centric and from predominantly static cameras, future work could evaluate how *TempO* pre-training behaves on a mixture of domains or highly repetitive videos, *e.g.* from an indoor service robot. Thirdly, the design of our proposed pretext task directly applies to models that output a set of proposal features. Keypoint-based detection methods or other models would require an additional tokenization strategy.

## 5. Conclusion

In this work, we proposed a SSL pretext task based on the temporal ordering of video frames, that allows learning region-level image representations. Models initialized with *TempO* pre-trained weights demonstrated a speed-up in convergence and superior performance on object detection and multi-object tracking downstream tasks compared to other self-supervised as well as supervised initialization strategies. The qualitative results also show how *TempO* pre-training helps to suppress ghost detection and recognize dark objects at night from a semantic context. In our multi-object tracking experiments, *TempO* pre-training improves the tracking accuracy while using a pre-trained object detector in a tracking-by-detection paradigm.

We, therefore, conclude that a temporal ordering pretext

task can boost performance compared to single-frame or supervised pre-training strategies in instance-level perception systems. We also evaluated the learned representations for a frame retrieval task, where we found consistent representations across videos of the same action class.

## References

- [1] Unaiza Ahsan, Rishi Madhok, and Irfan Essa. Video jigsaw: Unsupervised learning of spatiotemporal context for video action recognition. In *2019 IEEE Winter Conference on Applications of Computer Vision (WACV)*, pages 179–189. IEEE, 2019. 7
- [2] Borna Bešić, Nikhil Gosala, Daniele Cattaneo, and Abhinav Valada. Unsupervised domain adaptation for lidar panoptic segmentation. *IEEE Robotics and Automation Letters*, 7(2):3404–3411, 2022. 1
- [3] Nicolas Carion, Francisco Massa, Gabriel Synnaeve, Nicolas Usunier, Alexander Kirillov, and Sergey Zagoruyko. End-to-end object detection with transformers. In *European conference on computer vision*, pages 213–229. Springer, 2020. 3
- [4] Mathilde Caron, Ishan Misra, Julien Mairal, Priya Goyal, Piotr Bojanowski, and Armand Joulin. Unsupervised learning of visual features by contrasting cluster assignments. *Advances in Neural Information Processing Systems*, 33:9912–9924, 2020. 1, 2
- [5] Mathilde Caron, Hugo Touvron, Ishan Misra, Hervé Jégou, Julien Mairal, Piotr Bojanowski, and Armand Joulin. Emerging properties in self-supervised vision transformers. In *Proceedings of the International Conference on Computer Vision (ICCV)*, 2021. 1, 2, 5, 13
- [6] Ting Chen, Simon Kornblith, Mohammad Norouzi, and Geoffrey Hinton. A simple framework for contrastive learning of visual representations. In *International conference on machine learning*, pages 1597–1607. PMLR, 2020. 1, 2
- [7] Xinlei Chen, Haoqi Fan, Ross Girshick, and Kaiming He. Improved baselines with momentum contrastive learning. *arXiv preprint arXiv:2003.04297*, 2020. 2, 5, 13
- [8] Zhigang Dai, Bolun Cai, Yugeng Lin, and Junying Chen. Up-detr: Unsupervised pre-training for object detection with transformers. In *Proceedings of the IEEE/CVF Conference on Computer Vision and Pattern Recognition (CVPR)*, pages 1601–1610, June 2021. 1, 2, 5, 7
- [9] Jian Ding, Enze Xie, Hang Xu, Chenhan Jiang, Zhenguo Li, Ping Luo, and Guisong Xia. Deeply unsupervised patch re-identification for pre-training object detectors. *IEEE transactions on pattern analysis and machine intelligence*, PP, 2022. 2
- [10] Jian Ding, Enze Xie, Hang Xu, Chenhan Jiang, Zhenguo Li, Ping Luo, and Gui-Song Xia. Deeply unsupervised patch re-identification for pre-training object detectors. *IEEE Transactions on Pattern Analysis and Machine Intelligence*, 2022. 2
- [11] Christoph Feichtenhofer, Haoqi Fan, Bo Xiong, Ross Girshick, and Kaiming He. A large-scale study on unsupervised spatiotemporal representation learning. In *Proceedings of the IEEE/CVF Conference on Computer Vision and Pattern Recognition*, pages 3299–3309, 2021. 2
- [12] Basura Fernando, Hakan Bilen, Efstratios Gavves, and Stephen Gould. Self-supervised video representation learning with odd-one-out networks. In *Proceedings of the IEEE conference on computer vision and pattern recognition*, pages 3636–3645, 2017. 2
- [13] Whye Kit Fong, Rohit Mohan, Juana Valeria Hurtado, Lubing Zhou, Holger Caesar, Oscar Beijbom, and Abhinav Valada. Panoptic nusenes: A large-scale benchmark for lidar panoptic segmentation and tracking. *IEEE Robotics and Automation Letters*, 7(2):3795–3802, 2022. 1
- [14] Clément Godard, Oisín Mac Aodha, Michael Firman, and Gabriel J Brostow. Digging into self-supervised monocular depth estimation. In *Proceedings of the IEEE/CVF International Conference on Computer Vision*, pages 3828–3838, 2019. 1
- [15] Nikhil Gosala and Abhinav Valada. Bird’s-eye-view panoptic segmentation using monocular frontal view images. *IEEE Robotics and Automation Letters*, 7(2):1968–1975, 2022. 2
- [16] Jean-Bastien Grill, Florian Strub, Florent Altché, Corentin Tallec, Pierre Richemond, Elena Buchatskaya, Carl Doersch, Bernardo Avila Pires, Zhaohan Guo, Mohammad Gheshlaghi Azar, et al. Bootstrap your own latent—a new approach to self-supervised learning. *Advances in neural information processing systems*, 33:21271–21284, 2020. 1, 2
- [17] Tengda Han, Weidi Xie, and Andrew Zisserman. Self-supervised co-training for video representation learning. *Advances in Neural Information Processing Systems*, 33:5679–5690, 2020. 2
- [18] Kaiming He, Xiangyu Zhang, Shaoqing Ren, and Jian Sun. Deep residual learning for image recognition. In *Proceedings of the IEEE conference on computer vision and pattern recognition*, pages 770–778, 2016. 3, 4
- [19] Olivier J. H’énaff, Skanda Koppula, Jean-Baptiste Alayrac, Aäron van den Oord, Oriol Vinyals, and João Carreira. Efficient visual pretraining with contrastive detection. *2021 IEEE/CVF International Conference on Computer Vision (ICCV)*, pages 10066–10076, 2021. 2
- [20] Olivier J Hénaff, Skanda Koppula, Evan Shelhamer, Daniel Zoran, Andrew Jaegle, Andrew Zisserman, João Carreira, and Relja Arandjelović. Object discovery and representation networks. *arXiv preprint arXiv:2203.08777*, 2022. 2
- [21] Allan Jabri, Andrew Owens, and Alexei Efros. Space-time correspondence as a contrastive random walk. *Advances in neural information processing systems*, 33:19545–19560, 2020. 2
- [22] Arne Hoffhues Jonathon Luiten. Trackeval. <https://github.com/JonathonLuiten/TrackEval>, 2020. 5
- [23] Quan Kong, Wenpeng Wei, Ziwei Deng, Tomoaki Yoshinaga, and Tomokazu Murakami. Cycle-contrast for self-supervised video representation learning. *Advances in Neural Information Processing Systems*, 33:8089–8100, 2020. 1, 7
- [24] Christopher Lang, Alexander Braun, Lars Schillingmann, and Abhinav Valada. On hyperbolic embeddings in object detection. In *Pattern Recognition: 44th DAGM German Confer-*

- ence, *DAGM GCPR 2022, Konstanz, Germany, September 27–30, 2022, Proceedings*, pages 462–476. Springer, 2022. 2
- [25] Christopher Lang, Alexander Braun, and Abhinav Valada. Robust object detection using knowledge graph embeddings. In *Pattern Recognition: 44th DAGM German Conference, DAGM GCPR 2022, Konstanz, Germany, September 27–30, 2022, Proceedings*, pages 445–461. Springer, 2022. 2
- [26] Hsin-Ying Lee, Jia-Bin Huang, Maneesh Singh, and Ming-Hsuan Yang. Unsupervised representation learning by sorting sequences. In *Proceedings of the IEEE international conference on computer vision*, pages 667–676, 2017. 1, 3
- [27] Hsin-Ying Lee, Jia-Bin Huang, Maneesh Kumar Singh, and Ming-Hsuan Yang. Unsupervised representation learning by sorting sequence. In *IEEE International Conference on Computer Vision*, 2017. 7
- [28] Tsung-Yi Lin, Michael Maire, Serge Belongie, James Hays, Pietro Perona, Deva Ramanan, Piotr Dollár, and C Lawrence Zitnick. Microsoft coco: Common objects in context. In *European conference on computer vision*, pages 740–755. Springer, 2014. 5
- [29] Songtao Liu, Zeming Li, and Jian Sun. Self-emd: Self-supervised object detection without imagenet. *arXiv preprint arXiv:2011.13677*, 2020. 2
- [30] Ilya Loshchilov and Frank Hutter. Decoupled weight decay regularization. *arXiv preprint arXiv:1711.05101*, 2017. 12
- [31] Jonathon Luiten, Aljosa Osep, Patrick Dendorfer, Philip Torr, Andreas Geiger, Laura Leal-Taixé, and Bastian Leibe. Hota: A higher order metric for evaluating multi-object tracking. *International Journal of Computer Vision*, pages 1–31, 2020. 6
- [32] A. Milan, L. Leal-Taixé, I. Reid, S. Roth, and K. Schindler. MOT16: A benchmark for multi-object tracking. *arXiv:1603.00831 [cs]*, Mar. 2016. arXiv: 1603.00831. 4
- [33] Ishan Misra, C Lawrence Zitnick, and Martial Hebert. Shuffle and learn: unsupervised learning using temporal order verification. In *European conference on computer vision*, pages 527–544. Springer, 2016. 1, 2, 13
- [34] Rohit Mohan and Abhinav Valada. Amodal panoptic segmentation. In *Proceedings of the IEEE/CVF Conference on Computer Vision and Pattern Recognition*, pages 21023–21032, 2022. 2
- [35] Pedro O O Pinheiro, Amjad Almahairi, Ryan Benmalek, Florian Golemo, and Aaron C Courville. Unsupervised learning of dense visual representations. *Advances in Neural Information Processing Systems*, 33:4489–4500, 2020. 2
- [36] Jiangmiao Pang, Linlu Qiu, Xia Li, Haofeng Chen, Qi Li, Trevor Darrell, and Fisher Yu. Quasi-dense similarity learning for multiple object tracking. In *Proceedings of the IEEE/CVF conference on computer vision and pattern recognition*, pages 164–173, 2021. 4, 5, 7
- [37] AJ Piergiovanni, Anelia Angelova, and Michael S Ryoo. Evolving losses for unsupervised video representation learning. In *Proceedings of the IEEE/CVF Conference on Computer Vision and Pattern Recognition*, pages 133–142, 2020. 3
- [38] Pedro H. O. Pinheiro, Amjad Almahairi, Ryan Y. Benmalek, Florian Golemo, and Aaron C. Courville. Unsupervised learning of dense visual representations. *ArXiv*, abs/2011.05499, 2020. 2
- [39] Rui Qian, Tianjian Meng, Boqing Gong, Ming-Hsuan Yang, Huisheng Wang, Serge Belongie, and Yin Cui. Spatiotemporal contrastive video representation learning. In *Proceedings of the IEEE/CVF Conference on Computer Vision and Pattern Recognition*, pages 6964–6974, 2021. 2
- [40] Shuai Shao, Zijian Zhao, Boxun Li, Tete Xiao, Gang Yu, Xiangyu Zhang, and Jian Sun. Crowdhuman: A benchmark for detecting human in a crowd. *arXiv preprint arXiv:1805.00123*, 2018. 6
- [41] Khurram Soomro, Amir Roshan Zamir, and Mubarak Shah. Ucf101: A dataset of 101 human actions classes from videos in the wild. *arXiv preprint arXiv:1212.0402*, 2012. 7, 8
- [42] Peize Sun, Rufeng Zhang, Yi Jiang, Tao Kong, Chenfeng Xu, Wei Zhan, Masayoshi Tomizuka, Lei Li, Zehuan Yuan, Changhuo Wang, and Ping Luo. SparseR-CNN: End-to-end object detection with learnable proposals. *arXiv preprint arXiv:2011.12450*, 2020. 3, 4, 5, 12
- [43] Yonglong Tian, Dilip Krishnan, and Phillip Isola. Contrastive multiview coding. *arXiv preprint arXiv:1906.05849*, 2019. 2
- [44] Martine Toering, Ioannis Gatopoulos, Maarten Stol, and Vincent Tao Hu. Self-supervised video representation learning with cross-stream prototypical contrasting. *Proceedings of the IEEE/CVF Winter Conference on Applications of Computer Vision (WACV)*, 2022. 2
- [45] Abhinav Valada, Ankit Dhall, and Wolfram Burgard. Convolutional mixture of deep experts for robust semantic segmentation. In *IEEE/RSJ International conference on intelligent robots and systems (IROS) workshop, state estimation and terrain perception for all terrain mobile robots*, 2016. 2
- [46] Francisco Rivera Valverde, Juana Valeria Hurtado, and Abhinav Valada. There is more than meets the eye: Self-supervised multi-object detection and tracking with sound by distilling multimodal knowledge. In *Proceedings of the IEEE/CVF Conference on Computer Vision and Pattern Recognition*, pages 11612–11621, 2021. 1
- [47] Xiaolong Wang, Allan Jabri, and Alexei A Efros. Learning correspondence from the cycle-consistency of time. In *Proceedings of the IEEE/CVF Conference on Computer Vision and Pattern Recognition*, pages 2566–2576, 2019. 1, 2
- [48] Xinlong Wang, Rufeng Zhang, Chunhua Shen, Tao Kong, and Lei Li. Dense contrastive learning for self-supervised visual pre-training. In *Proceedings of the IEEE/CVF Conference on Computer Vision and Pattern Recognition*, pages 3024–3033, 2021. 2
- [49] Donglai Wei, Joseph J Lim, Andrew Zisserman, and William T Freeman. Learning and using the arrow of time. In *Proceedings of the IEEE Conference on Computer Vision and Pattern Recognition*, pages 8052–8060, 2018. 2, 3
- [50] Olivia Wiles, Joao Carreira, Iain Barr, Andrew Zisserman, and Mateusz Malinowski. Compressed vision for efficient video understanding. *arXiv preprint arXiv:2210.02995*, 2022. 8

- [51] Enze Xie, Jian Ding, Wenhai Wang, Xiaohang Zhan, Hang Xu, Zhenguo Li, and Ping Luo. Detco: Unsupervised contrastive learning for object detection. *2021 IEEE/CVF International Conference on Computer Vision (ICCV)*, pages 8372–8381, 2021. 2
- [52] Zhenda Xie, Yutong Lin, Zheng Zhang, Yue Cao, Stephen Lin, and Han Hu. Propagate yourself: Exploring pixel-level consistency for unsupervised visual representation learning. In *Proceedings of the IEEE/CVF Conference on Computer Vision and Pattern Recognition*, pages 16684–16693, 2021. 1, 2
- [53] Dejing Xu, Jun Xiao, Zhou Zhao, Jian Shao, Di Xie, and Yueting Zhuang. Self-supervised spatiotemporal learning via video clip order prediction. In *Proceedings of the IEEE/CVF Conference on Computer Vision and Pattern Recognition*, pages 10334–10343, 2019. 2, 5, 13
- [54] Ceyuan Yang, Zhirong Wu, Bolei Zhou, and Stephen Lin. Instance localization for self-supervised detection pretraining. In *Proceedings of the IEEE/CVF Conference on Computer Vision and Pattern Recognition*, pages 3987–3996, 2021. 2
- [55] Junwei Yang, Ke Zhang, Zhaolin Cui, Jinming Su, Junfeng Luo, and Xiaolin Wei. Inscon: Instance consistency feature representation via self-supervised learning. *arXiv preprint arXiv:2203.07688*, 2022. 2
- [56] Fisher Yu, Haofeng Chen, Xin Wang, Wenqi Xian, Yingying Chen, Fangchen Liu, Vashisht Madhavan, and Trevor Darrell. Bdd100k: A diverse driving dataset for heterogeneous multi-task learning. In *Proceedings of the IEEE/CVF conference on computer vision and pattern recognition*, pages 2636–2645, 2020. 1, 4
- [57] Yucheng Zhao, Guangting Wang, Chong Luo, Wenjun Zeng, and Zhengjun Zha. Self-supervised visual representations learning by contrastive mask prediction. *2021 IEEE/CVF International Conference on Computer Vision (ICCV)*, pages 10140–10149, 2021. 2
- [58] Xizhou Zhu, Weijie Su, Lewei Lu, Bin Li, Xiaogang Wang, and Jifeng Dai. Deformable detr: Deformable transformers for end-to-end object detection. *arXiv preprint arXiv:2010.04159*, 2020. 3

# Self-Supervised Representation Learning from Temporal Ordering of Automated Driving Sequences

## - Supplementary Material -

Christopher Lang<sup>1,2</sup>   Alexander Braun<sup>2</sup>   Lars Schillingmann<sup>2</sup>   Karsten Haug<sup>2</sup>   Abhinav Valada<sup>1</sup>  
<sup>1</sup>University of Freiburg   <sup>2</sup>Robert Bosch GmbH

In this supplementary material, we provide additional insights and experimental results on knowledge embedding-based object detection.

---

### Algorithm 1: TempO pretext task pipeline.

---

**Data:** Image sequence  $\mathcal{I}_1, \dots, \mathcal{I}_N$  in correct temporal order, margin  $m$   
**Result:**  $\mathcal{L}_{TempO}$

```

1 forall  $\mathcal{I}_i$  do
2    $\mathcal{T}_i = \text{SpatialNetwork}(\mathcal{I}_i)$ 
3 end
4 # per-frame track tokens  $\mathbf{T}_i \in \mathbb{R}^{Q \times D}$ ;
5  $\mathbf{H}_{1:N-1} = \text{HistoryEncoder}([\mathcal{T}_1, \dots, \mathcal{T}_{N-1}], \mathcal{M}_{future})$ ;
6 # history tokens  $\mathbf{H}_{1:N-1} \in \mathbb{R}^{(N-1) \cdot Q \times D}$ ;
7  $\mathcal{L}_{TempO} = 0$ ;
8 for  $i \in [2, \dots, N]$  do
9   # matching scores  $\mathbf{S}_i \in \mathbb{R}^{(N-i-1) \times P \times P}$ ;
10   $\mathbf{S}_{i,i-1} = \text{AdditiveAttention}(\mathbf{T}_i, \mathbf{H}_{i-1})$ ;
11   $p_{i,i-1} = \text{ReductionFunction}(\mathbf{S}_{i,i-1})$ ;
12  for  $j \in [1, \dots, N-1]$  &  $j \neq i-1$  do
13     $\mathbf{S}_{i,j} = \text{AdditiveAttention}(\mathbf{T}_i, \mathbf{H}_j)$ ;
14     $n_{i,j} = \text{ReductionFunction}(\mathbf{S}_{i,j})$ ;
15     $\mathcal{L}_{TempO} += \max\{n_{i,j} - p_{i,i-1} + m, 0\}$ 
16  end
17 end

```

---

## 1. Convergence Experiments

In Table 1, we compare the object detection performance of different initialization strategies over the number of fine-tuning epochs. All models were trained using NVIDIA V100 GPUs with a batch size of 16 for 12 epochs on the BDD100K train split. We use the AdamW [30] optimizer with an initial learning rate of  $2.5 \cdot 10^{-5}$  and weight decay of  $10^{-4}$ , and reduced the learning rate by a factor of 10 after 8 epochs.

We observe that the *TempO* pretrained initialization yields the fastest convergence and achieves the largest mean average precision among different initialization strategies from 3 fine-tuning epochs onwards. As a result, the *TempO* pre-trained models fine-tuned for 6 epochs achieve comparable results to COCO 2017 pre-trained methods for 12 fine-tuning epochs and surpass COCO 2017 pre-trained initial-

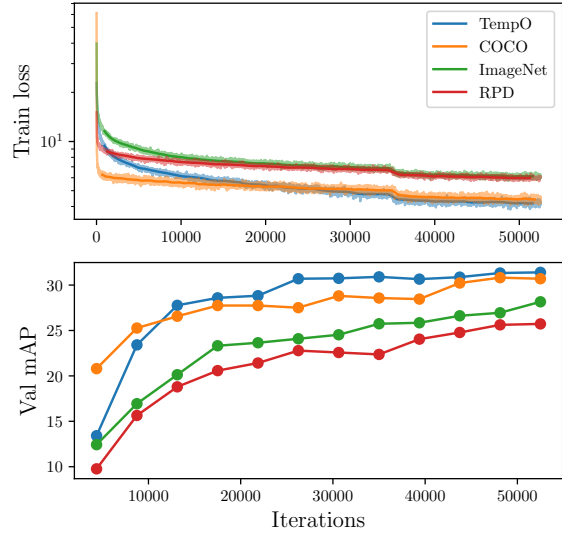


Figure 1. Training loss and validation set mAP for varying initialization strategies for a Sparse R-CNN object detector over 6 fine-tuning epochs on the BDD100K dataset. We train with a batch size of 16, and decrease the learning rate by a factor of 10 after 8 epochs (35k iterations).

ization by more than +0.7% after 12 fine-tuning epochs. Noticeably, the detection performance for large and medium-sized objects increases at a high rate during the early fine-tuning epochs of *TempO*, but slows down after 6 epochs compared to COCO 2017 initialized detectors. However, the performance at this stage is already higher than that achieved by the COCO 2017 initialized object detectors.

Figure 1 presents the loss per epoch for fine-tuning a Sparse R-CNN [42] object detector on the BDD100K dataset using varying initialization strategies. We observe that the *TempO* pretrained method’s detection performance increases the fastest at the early training epochs, and achieves the highest detection performance throughout the second half of the fine-tuning epochs. Analogous to Table 1, the improvement in the mAP metric slows down for *TempO* pretrained methods after 6 fine-tuning epochs, while the remaining initialization strategies have still not converged. These results

Table 1. Object detection results on the BDD100k val set for increasing number of fine-tuning epochs. The *TempO* pre-training uses a sequence length of 8 frames, two layers in the multi-frame network, and AvgPool motivated by Table 3 in the main paper.

Model	Pretrain	Epoch	BDD100k val object detection					
			AP	AP50	AP75	APs	APm	API
SparseRCNN	COCO	2	25.3	47.6	23.1	12.5	28.4	40.3
		4	27.7	51.0	25.8	13.7	31.2	44.5
		6	27.5	49.9	25.8	12.6	30.5	47.8
		12	30.7	55.8	28.9	15.2	34.3	50.8
SparseRCNN	TempO	2	23.4	46.0	20.8	11.0	27.0	36.2
		4	28.6	52.5	26.9	13.6	32.4	48.3
		6	30.7	55.5	28.6	15.4	34.6	49.6
		12	31.4	57.2	29.3	15.3	35.2	52.4
DDETR	COCO	2	9.3	20.9	6.9	4.5	11.6	17.3
		4	16.8	34.7	14	7.6	19.8	30.6
		6	28.3	52.2	26.1	11.2	32.1	53.6
		12	30.2	56.0	27.6	14.2	34.0	51.3
DDETR	TempO	2	13.9	29.9	11.3	6.1	16.6	26.6
		4	30.6	55.9	28.3	12.7	34.3	55.0
		6	31.3	57.9	28.9	15.2	34.9	55.3
		12	<b>32.5</b>	<b>59.2</b>	<b>30.4</b>	<b>15.7</b>	<b>36.9</b>	<b>55.3</b>

Table 2. Object detection results using Sparse R-CNN model on the BDD100k val dataset. All methods use a ResNet-50 backbone.

Pre-train Method	BDD100k val object detection					
	AP	AP50	AP75	APs	APm	API
COCO (supervised)	27.5	49.9	25.8	12.6	30.5	47.8
MoCo v2 [7]	24.8	46.7	22.4	12.7	28.3	39.1
DINO [5]	26.7	50.0	24.3	13.0	29.9	46.1
Frame order verification [33]	27.4	51.1	25.0	13.8	31.3	43.5
Frame order classification [53]	27.0	49.7	24.8	12.3	30.5	46.2
TempO (Ours)	<b>30.7</b>	<b>55.5</b>	<b>28.6</b>	<b>15.4</b>	<b>34.6</b>	<b>49.6</b>

demonstrate that the *TempO* pre-trained models converge faster than other pre-training strategies.

## 2. Object Detection Performance of Scene-level SSL Methods

We found pre-training on methods that learn scene-level feature descriptors only partially comparable with our approach, since the parameters of the object detector neck and head are not initialized with the SSL pretrained weights. However, we cannot quantify the effect that the choice of initialization strategy for those parameters has on the evaluation after fine-tuning.

In Table 2, we present such comparisons with SSL methods that incorporate self-supervised scene-level feature learning strategies from frame-based [5, 7] and sequence-based [33, 53] pretext tasks. We trained the single-frame methods on double bounding box crops from the BDD100k detection train set, and the sequence-based methods on the same dataset as our *TempO* method, using the training protocol described in Sec. 4.2 of the manuscript. For frame order verification and classification, we used a sequence length of 3 and 5, respectively.

The experiments in Table 2 in the following with use a random parameter initialization for the detector neck and head. We observe that our *TempO* approach outperforms all the strategies using scene-level SSL methods for initializing the ResNet-50 backbone and random initialization for the remaining network parameters by  $\geq +3.3\%$  in mAP on the BDD100k validation set. This amends the experiments in the main paper, which showed that our proposed approach also outperforms initialization strategies that pretrain all detector parameters, *e.g.* from supervised training on the COCO 2017 dataset or self-supervised training on re-localization of random image patches.